2011

Suppression Of Away-Side Jet Fragments With Respect To The Reaction Plane In Au + Au Collisions At √sNN=200 GeV

Andrew Marshall Adare

Gyöngyi Baksay

László A. Baksay

Szabolcs Rembeczki

Marcus Hohlmann

Suppression of away-side jet fragments with respect to the reaction plane in Au + Au collisions at $\sqrt{s_{NN}} = 200$ GeV

A. Adare,[1] S. Afanasiev,[2] C. Aidala,[3] N. N. Ajitanand,[4] Y. Akiba,[5,6] H. Al-Bataineh,[7] J. Alexander,[4] K. Aoki,[8,5] L. Aphecetche,[9] Y. Aramaki,[10] J. Asai,[5] E. T. Atomssa,[11] R. Averbeck,[12] T. C. Awes,[13] B. Azmoun,[14] V. Babintsev,[15] M. Bai,[16] G. Baksay,[17] L. Baksay,[17] A. Baldisseri,[18] K. N. Barish,[19] P. D. Barnes,[20,*] B. Bassalleck,[21] A. T. Basye,[22] S. Bathe,[19] S. Batsouli,[13] V. Baublis,[23] C. Baumann,[24] A. Bazilevsky,[14] S. Belikov,[14,*] R. Belmont,[25] R. Bennett,[12] A. Berdnikov,[26] Y. Berdnikov,[26] A. A. Bickley,[1] J. G. Boissevain,[20] J. S. Bok,[27] H. Borel,[18] K. Boyle,[12] M. L. Brooks,[20] H. Buesching,[14] V. Bumazhnov,[15] G. Bunce,[14,16] S. Butsyk,[20] C. M. Camacho,[20] S. Campbell,[12] B. S. Chang,[27] W. C. Chang,[28] J.-L. Charvet,[18] C.-H. Chen,[12] S. Chernichenko,[15] C. Y. Chi,[29] M. Chiu,[14,30] I. J. Choi,[27] R. K. Choudhury,[31] P. Christiansen,[32] T. Chujo,[33] P. Chung,[4] A. Churyn,[15] O. Chvala,[19] V. Cianciolo,[13] Z. Citron,[12] B. A. Cole,[29] M. Connors,[12] P. Constantin,[20] M. Csanád,[34] T. Csörgő,[35] T. Dahms,[12] S. Dairaku,[8,5] I. Danchev,[25] K. Das,[36] A. Datta,[3] G. David,[14] A. Denisov,[15] D. d'Enterria,[11] A. Deshpande,[6,12] E. J. Desmond,[14] O. Dietzsch,[37] A. Dion,[12] M. Donadelli,[37] O. Drapier,[11] A. Drees,[12] K. A. Drees,[16] A. K. Dubey,[38] J. M. Durham,[12] A. Durum,[15] D. Dutta,[31] V. Dzhordzhadze,[19] S. Edwards,[36] Y. V. Efremenko,[13] F. Ellinghaus,[1] T. Engelmore,[29] A. Enokizono,[39] H. En'yo,[5,6] S. Esumi,[33] K. O. Eyser,[19] B. Fadem,[40] D. E. Fields,[21,6] M. Finger,[41] M. Finger Jr.,[41] F. Fleuret,[11] S. L. Fokin,[42] Z. Fraenkel,[38,*] J. E. Frantz,[12] A. Franz,[14] A. D. Frawley,[36] K. Fujiwara,[5] Y. Fukao,[8,5] T. Fusayasu,[43] I. Garishvili,[44] A. Glenn,[1] H. Gong,[12] M. Gonin,[11] J. Gosset,[18] Y. Goto,[5,6] R. Granier de Cassagnac,[11] N. Grau,[29] S. V. Greene,[25] M. Grosse Perdekamp,[30,6] T. Gunji,[10] H.-Å. Gustafsson,[32,*] A. Hadj Henni,[9] J. S. Haggerty,[14] K. I. Hahn,[45] H. Hamagaki,[10] J. Hamblen,[44] R. Han,[46] J. Hanks,[29] E. P. Hartouni,[39] K. Haruna,[47] E. Haslum,[32] R. Hayano,[10] X. He,[48] M. Heffner,[39] T. K. Hemmick,[12] T. Hester,[19] J. C. Hill,[49] M. Hohlmann,[17] W. Holzmann,[29,4] K. Homma,[47] B. Hong,[50] T. Horaguchi,[10,47,5,51] D. Hornback,[44] S. Huang,[25] T. Ichihara,[5,6] R. Ichimiya,[5] J. Ide,[40] H. Iinuma,[8,5] Y. Ikeda,[33] K. Imai,[8,5] J. Imrek,[52] M. Inaba,[33] D. Isenhower,[22] M. Ishihara,[5] T. Isobe,[10] M. Issah,[4,25] A. Isupov,[2] D. Ivanischev,[23] B. V. Jacak,[12,†] J. Jia,[14,29,4] J. Jin,[29] B. M. Johnson,[14] K. S. Joo,[53] D. Jouan,[54] D. S. Jumper,[22] F. Kajihara,[10] S. Kametani,[5] N. Kamihara,[6] J. Kamin,[12] J. H. Kang,[27] J. Kapustinsky,[20] K. Karatsu,[8] D. Kawall,[3,6] M. Kawashima,[55,5] A. V. Kazantsev,[42] T. Kempel,[49] A. Khanzadeev,[23] K. M. Kijima,[47] J. Kikuchi,[56] B. I. Kim,[50] D. H. Kim,[53] D. J. Kim,[57,27] E. Kim,[58] E. J. Kim,[59] S. H. Kim,[27] Y. J. Kim,[30] E. Kinney,[1] K. Kiriluk,[1] Á. Kiss,[34] E. Kistenev,[14] J. Klay,[39] C. Klein-Boesing,[24] L. Kochenda,[23] B. Komkov,[23] M. Konno,[33] J. Koster,[30] D. Kotchetkov,[21] A. Kozlov,[38] A. Král,[60] A. Kravitz,[29] G. J. Kunde,[20] K. Kurita,[55,5] M. Kurosawa,[5] M. J. Kweon,[50] Y. Kwon,[44,27] G. S. Kyle,[7] R. Lacey,[4] Y. S. Lai,[29] J. G. Lajoie,[49] D. Layton,[30] A. Lebedev,[49] D. M. Lee,[20] J. Lee,[45] K. Lee,[58] K. B. Lee,[50] K. S. Lee,[50] T. Lee,[58] M. J. Leitch,[20] M. A. L. Leite,[37] E. Leitner,[25] B. Lenzi,[37] X. Li,[61] P. Liebing,[6] L. A. Linden Levy,[1] T. Liška,[60] A. Litvinenko,[2] H. Liu,[20,7] M. X. Liu,[20] B. Love,[25] R. Luechtenborg,[24] D. Lynch,[14] C. F. Maguire,[25] Y. I. Makdisi,[16] A. Malakhov,[2] M. D. Malik,[21] V. I. Manko,[42] E. Mannel,[29] Y. Mao,[46,5] L. Mašek,[41,62] H. Masui,[33] F. Matathias,[29] M. McCumber,[12] P. L. McGaughey,[20] N. Means,[12] B. Meredith,[30] Y. Miake,[33] A. C. Mignerey,[63] P. Mikeš,[41,62] K. Miki,[33] A. Milov,[14] M. Mishra,[64] J. T. Mitchell,[14] A. K. Mohanty,[31] Y. Morino,[10] A. Morreale,[19] D. P. Morrison,[14] T. V. Moukhanova,[42] D. Mukhopadhyay,[25] J. Murata,[55,5] S. Nagamiya,[65] J. L. Nagle,[1] M. Naglis,[38] M. I. Nagy,[34] I. Nakagawa,[5,6] Y. Nakamiya,[47] T. Nakamura,[47,65] K. Nakano,[5,51] J. Newby,[39] M. Nguyen,[12] T. Niita,[33] R. Nouicer,[14] A. S. Nyanin,[42] E. O'Brien,[14] S. X. Oda,[10] C. A. Ogilvie,[49] M. Oka,[33] K. Okada,[6] Y. Onuki,[5] A. Oskarsson,[32] M. Ouchida,[47] K. Ozawa,[10] R. Pak,[14] A. P. T. Palounek,[20] V. Pantuev,[66,12] V. Papavassiliou,[7] I. H. Park,[45] J. Park,[58] S. K. Park,[50] W. J. Park,[50] S. F. Pate,[7] H. Pei,[49] J.-C. Peng,[30] H. Pereira,[18] V. Peresedov,[2] D. Yu. Peressounko,[42] C. Pinkenburg,[14] R. P. Pisani,[14] M. Proissl,[12] M. L. Purschke,[14] A. K. Purwar,[20] H. Qu,[48] J. Rak,[57,21] A. Rakotozafindrabe,[11] I. Ravinovich,[38] K. F. Read,[13,44] S. Rembeczki,[17] K. Reygers,[24] V. Riabov,[23] Y. Riabov,[23] E. Richardson,[63] D. Roach,[25] G. Roche,[67] S. D. Rolnick,[19] M. Rosati,[49] C. A. Rosen,[1] S. S. E. Rosendahl,[32] P. Rosnet,[67] P. Rukoyatkin,[2] P. Ružička,[62] V. L. Rykov,[5] B. Sahlmueller,[24] N. Saito,[65,8,5,6] T. Sakaguchi,[14] S. Sakai,[33] K. Sakashita,[5,51] V. Samsonov,[23] S. Sano,[10,56] T. Sato,[33] S. Sawada,[65] K. Sedgwick,[19] J. Seele,[1] R. Seidl,[30] A. Yu. Semenov,[49] V. Semenov,[15] R. Seto,[19] D. Sharma,[38] I. Shein,[15] T.-A. Shibata,[5,51] K. Shigaki,[47] M. Shimomura,[33] K. Shoji,[8,5] P. Shukla,[31] A. Sickles,[14] C. L. Silva,[37] D. Silvermyr,[13] C. Silvestre,[18] K. S. Sim,[50] B. K. Singh,[64] C. P. Singh,[64] V. Singh,[64] M. Slunečka,[41] A. Soldatov,[15] R. A. Soltz,[39] W. E. Sondheim,[20] S. P. Sorensen,[44] I. V. Sourikova,[14] N. A. Sparks,[22] F. Staley,[18] P. W. Stankus,[13] E. Stenlund,[32] M. Stepanov,[7] A. Ster,[35] S. P. Stoll,[14] T. Sugitate,[47] C. Suire,[54] A. Sukhanov,[14] J. Sziklai,[35] E. M. Takagui,[37] A. Taketani,[5,6] R. Tanabe,[33] Y. Tanaka,[43] K. Tanida,[8,5,6,58] M. J. Tannenbaum,[14] S. Tarafdar,[64] A. Taranenko,[4] P. Tarján,[52] H. Themann,[12] T. L. Thomas,[21] M. Togawa,[8,5] A. Toia,[12] L. Tomášek,[62] Y. Tomita,[33] H. Torii,[47,5] R. S. Towell,[22] V-N. Tram,[11] I. Tserruya,[38] Y. Tsuchimoto,[47] C. Vale,[14,49] H. Valle,[25] H. W. van Hecke,[20] E. Vazquez-Zambrano,[29] A. Veicht,[30] J. Velkovska,[25] R. Vértesi,[52,35] A. A. Vinogradov,[42] M. Virius,[60] V. Vrba,[62] E. Vznuzdaev,[23] X. R. Wang,[7] D. Watanabe,[47] K. Watanabe,[33] Y. Watanabe,[5,6] F. Wei,[49] R. Wei,[4] J. Wessels,[24] S. N. White,[14] D. Winter,[29] J. P. Wood,[22] C. L. Woody,[14] R. M. Wright,[22] M. Wysocki,[1] W. Xie,[6] Y. L. Yamaguchi,[10,56] K. Yamaura,[47] R. Yang,[30] A. Yanovich,[15] J. Ying,[48] S. Yokkaichi,[5,6] Z. You,[46] G. R. Young,[13] I. Younus,[21] I. E. Yushmanov,[42] W. A. Zajc,[29] O. Zaudtke,[24] C. Zhang,[13] S. Zhou,[61] and L. Zolin[2]

(PHENIX Collaboration)

[1]*University of Colorado, Boulder, Colorado 80309, USA*
[2]*Joint Institute for Nuclear Research, 141980 Dubna, Moscow Region, Russia*
[3]*Department of Physics, University of Massachusetts, Amherst, Massachusetts 01003-9337, USA*
[4]*Chemistry Department, Stony Brook University, SUNY, Stony Brook, New York 11794-3400, USA*
[5]*RIKEN Nishina Center for Accelerator-Based Science, Wako, Saitama 351-0198, Japan*
[6]*RIKEN BNL Research Center, Brookhaven National Laboratory, Upton, New York 11973-5000, USA*
[7]*New Mexico State University, Las Cruces, New Mexico 88003, USA*
[8]*Kyoto University, Kyoto 606-8502, Japan*
[9]*SUBATECH (Ecole des Mines de Nantes, CNRS-IN2P3, Université de Nantes) BP 20722, F-44307, Nantes, France*
[10]*Center for Nuclear Study, Graduate School of Science, University of Tokyo, 7-3-1 Hongo, Bunkyo, Tokyo 113-0033, Japan*
[11]*Laboratoire Leprince-Ringuet, Ecole Polytechnique, CNRS-IN2P3, Route de Saclay, F-91128, Palaiseau, France*
[12]*Department of Physics and Astronomy, Stony Brook University, SUNY, Stony Brook, New York 11794-3400, USA*
[13]*Oak Ridge National Laboratory, Oak Ridge, Tennessee 37831, USA*
[14]*Physics Department, Brookhaven National Laboratory, Upton, New York 11973-5000, USA*
[15]*IHEP Protvino, State Research Center of Russian Federation, Institute for High Energy Physics, Protvino, 142281, Russia*
[16]*Collider-Accelerator Department, Brookhaven National Laboratory, Upton, New York 11973-5000, USA*
[17]*Florida Institute of Technology, Melbourne, Florida 32901, USA*
[18]*Dapnia, CEA Saclay, F-91191, Gif-sur-Yvette, France*
[19]*University of California Riverside, Riverside, California 92521, USA*
[20]*Los Alamos National Laboratory, Los Alamos, New Mexico 87545, USA*
[21]*University of New Mexico, Albuquerque, New Mexico 87131, USA*
[22]*Abilene Christian University, Abilene, Texas 79699, USA*
[23]*PNPI, Petersburg Nuclear Physics Institute, Gatchina, Leningrad region, 188300, Russia*
[24]*Institut fur Kernphysik, University of Muenster, D-48149 Muenster, Germany*
[25]*Vanderbilt University, Nashville, Tennessee 37235, USA*
[26]*Saint Petersburg State Polytechnic University, St. Petersburg, 195251 Russia*
[27]*Yonsei University, IPAP, Seoul 120-749, Korea*
[28]*Institute of Physics, Academia Sinica, Taipei 11529, Taiwan*
[29]*Columbia University, New York, New York 10027 and Nevis Laboratories, Irvington, New York 10533, USA*
[30]*University of Illinois at Urbana-Champaign, Urbana, Illinois 61801, USA*
[31]*Bhabha Atomic Research Centre, Bombay 400 085, India*
[32]*Department of Physics, Lund University, Box 118, S-221 00 Lund, Sweden*
[33]*Institute of Physics, University of Tsukuba, Tsukuba, Ibaraki 305, Japan*
[34]*ELTE, Eötvös Loránd University, H-1117 Budapest, Pázmány P. s. 1/A, Hungary*
[35]*KFKI Research Institute for Particle and Nuclear Physics of the Hungarian Academy of Sciences (MTA KFKI RMKI), H-1525 Budapest 114, PO Box 49, Budapest, Hungary*
[36]*Florida State University, Tallahassee, Florida 32306, USA*
[37]*Universidade de São Paulo, Instituto de Física, Caixa Postal 66318, São Paulo CEP 05315-970, Brazil*
[38]*Weizmann Institute, Rehovot 76100, Israel*
[39]*Lawrence Livermore National Laboratory, Livermore, California 94550, USA*
[40]*Muhlenberg College, Allentown, Pennsylvania 18104-5586, USA*
[41]*Charles University, Ovocný trh 5, Praha 1, CZ-116 36, Prague, Czech Republic*
[42]*Russian Research Center "Kurchatov Institute", Moscow, 123098 Russia*
[43]*Nagasaki Institute of Applied Science, Nagasaki-shi, Nagasaki 851-0193, Japan*
[44]*University of Tennessee, Knoxville, Tennessee 37996, USA*
[45]*Ewha Womans University, Seoul 120-750, Korea*
[46]*Peking University, Beijing 100871, P. R. China*
[47]*Hiroshima University, Kagamiyama, Higashi-Hiroshima 739-8526, Japan*
[48]*Georgia State University, Atlanta, Georgia 30303, USA*
[49]*Iowa State University, Ames, Iowa 50011, USA*
[50]*Korea University, Seoul, 136-701, Korea*
[51]*Department of Physics, Tokyo Institute of Technology, Oh-okayama, Meguro, Tokyo 152-8551, Japan*
[52]*Debrecen University, H-4010 Debrecen, Egyetem tér 1, Hungary*
[53]*Myongji University, Yongin, Kyonggido 449-728, Korea*
[54]*IPN-Orsay, Universite Paris Sud, CNRS-IN2P3, BP1, F-91406, Orsay, France*
[55]*Physics Department, Rikkyo University, 3-34-1 Nishi-Ikebukuro, Toshima, Tokyo 171-8501, Japan*
[56]*Waseda University, Advanced Research Institute for Science and Engineering, 17 Kikui-cho, Shinjuku-ku, Tokyo 162-0044, Japan*
[57]*Helsinki Institute of Physics and University of Jyväskylä, P.O.Box 35, FIN-40014 Jyväskylä, Finland*

[58]*Seoul National University, Seoul, Korea*
[59]*Chonbuk National University, Jeonju, 561-756, Korea*
[60]*Czech Technical University, Zikova 4, CZ-166 36 Prague 6, Czech Republic*
[61]*Science and Technology on Nuclear Data Laboratory, China Institute of Atomic Energy, Beijing 102413, P. R. China*
[62]*Institute of Physics, Academy of Sciences of the Czech Republic, Na Slovance 2, CZ-182 21 Prague 8, Czech Republic*
[63]*University of Maryland, College Park, Maryland 20742, USA*
[64]*Department of Physics, Banaras Hindu University, Varanasi 221005, India*
[65]*KEK, High Energy Accelerator Research Organization, Tsukuba, Ibaraki 305-0801, Japan*
[66]*Institute for Nuclear Research of the Russian Academy of Sciences, prospekt 60-letiya Oktyabrya 7a, Moscow 117312, Russia*
[67]*LPC, Université Blaise Pascal, CNRS-IN2P3, Clermont-Fd, F-63177 Aubiere Cedex, France*
(Received 8 October 2010; revised manuscript received 7 July 2011; published 9 August 2011)

Pair correlations between large transverse momentum neutral pion triggers ($p_T = 4$–7 GeV/c) and charged hadron partners ($p_T = 3$–7 GeV/c) in central (0%–20%) and midcentral (20%–60%) Au + Au collisions at $\sqrt{s_{NN}} = 200$ GeV are presented as a function of trigger orientation with respect to the reaction plane. The particles are at larger momentum than where jet shape modifications have been observed, and the correlations are sensitive to the energy loss of partons traveling through hot dense matter. An out-of-plane trigger particle produces only $26 \pm 20\%$ of the away-side pairs that are observed opposite of an in-plane trigger particle for midcentral (20%–60%) collisions. In contrast, near-side jet fragments are consistent with no suppression or dependence on trigger orientation with respect to the reaction plane. These observations are qualitatively consistent with a picture of little near-side parton energy loss either due to surface bias or fluctuations and increased away-side parton energy loss due to a long path through the medium. The away-side suppression as a function of reaction-plane angle is shown to be sensitive to both the energy loss mechanism and the space-time evolution of heavy-ion collisions.

DOI: 10.1103/PhysRevC.84.024904 PACS number(s): 25.75.Nq, 25.75.Bh

I. INTRODUCTION

Collisions of heavy nuclei at the Relativistic Heavy Ion Collider have created matter with energy densities exceeding the predicted threshold for deconfinement of color charge into a hot dense plasma [1]. In this quark gluon plasma (QGP), quarks and gluons are not bound within hadronic states and the matter behaves collectively. Comparisons with hydrodynamic simulations indicate rapid thermalization of the colliding system into a hot dense nuclear medium. The produced medium affords an opportunity to study the properties of a new phase of quantum chromodynamics (QCD) in an extreme environment.

Hard scattering with large momentum exchange between partons in the incoming nuclei is well-described by perturbative QCD (pQCD). The scattered partons emerge back-to-back in azimuth in the plane transverse to the beam direction, and fragment into a pair of correlated cones of high momentum particles, referred to as jets. The study of jets and their hadronic fragments in heavy-ion collisions provides insight into the properties of hot dense nuclear matter. Measurements of single high transverse momentum (p_T) particles [2] and correlations between high-p_T particles [3–5] have demonstrated that the fast partons embedded in the produced medium dissipate a large amount of their initial kinetic energy.

In this paper we present angular correlations of hadron pairs with both hadrons in the midrapidity range $|\eta| < 0.35$. Fragments from the same jet form a peak at small relative azimuthal angle ($\Delta\phi$), that is, the near-side peak. Pairs composed of one fragment from each jet will appear in an away-side peak at $\Delta\phi \sim \pi$. Past measurements [3–5] for hadrons $\gtrsim 5$ GeV/c have shown that the away-side correlations peak is suppressed relative to baseline measurements in $p + p$ collisions. The suppression of the away-side jet is a signature of parton energy loss inside the medium. The same measurements show that near-side jet fragments at large momentum are not suppressed. This feature of the data is understood to result from the requirement of a large momentum particle in the final state, which creates a bias toward small energy loss either by the preferential selection of hard scatterings near the medium surface [6] or due to fluctuations in energy loss [7].

The detailed mechanism by which partons lose energy when passing through a deconfined medium are not yet fully understood. In pQCD descriptions of the parton-medium interaction the predicted parton energy loss should scale as the path length squared [8]. In competing anti-de-Sitter space and conformal field theory descriptions characterizing a strongly coupled medium, the energy loss scales as the path length cubed [8]. The variation in azimuthal angle of the away-side jet suppression with respect to the reaction plane (ϕ_s) is sensitive to the total amount of energy lost by the away-side parton along long paths (out-of-plane) or short paths (in-plane) through the medium. The degree to which the away-side jet suppression varies will be determined in part by the path-length scale of energy loss.

Single particle observables at high p_T, such as the nuclear suppression with respect to the reaction plane [$R_{AA}(\phi_s)$] or the azimuthal anisotropy (i.e., v_2) [9], are also sensitive to this path-length variation of energy loss. Current pQCD

*Deceased
†PHENIX Spokesperson:jacak@skipper.physics.sunysb.edu

calculations predict a lower v_2 than is found in the data and may imply a larger than path length squared dependence to energy loss [10,11]. The reaction-plane dependence of the back-to-back jets provides an additional test on the path length dependence in that the two particle observable selects a different distribution of hard-scattering locations and should probe longer paths through the medium than single particle observables. The path-length dependence of both single and two particle observables have already been studied through selection of the collision centrality [4,9]. However, centrality selection varies not only the path length, but also other important properties of the medium (e.g., the overall energy density). Selection with respect to the reaction plane more directly varies the path lengths, while leaving the other medium properties unchanged.

In addition to the uncertainties associated with the energy loss mechanisms, many of the details within hydrodynamic simulations of heavy-ion collisions have not been fully constrained and tested by experiment. For instance, one such uncertainty is the geometrical description of the energy deposited by the colliding nuclei which could contribute to the degree of away-side suppression variation with respect to the reaction plane. Two competing descriptions, the Glauber model [12] and the color glass condensate [13], predict different azimuthal distributions of matter with respect to the reaction plane. Thus the two descriptions give different in-plane and out-of-plane path lengths through the medium. These descriptions are also used as different starting points to the hydrodynamic evolution of the medium. Other model uncertainties include, but are not limited to, the extent of geometry fluctuations, the time required for thermalization into a hydrodynamic medium, the characteristics of the phase transition to confined hadrons, and the conditions under which those hadrons become free-streaming particles into the vacuum. These ambiguities in the proper modeling of heavy-ion collisions can result in significant uncertainty in the extracted properties of the medium, such as the shear viscosity [14].

In midcentral (the middle 20%–60% of the total cross section) collisions the variation of the away-side suppression is expected to be largest as the collision zone is the most anisotropic. In contrast, central (0%–20%) collisions are much more isotropic and so provide a sample of events with small anisotropy expected in the away-side suppression. For instance, in the Glauber model, midcentral events will have a root-mean-square thickness through the medium of 3.2 fm in the in-plane direction versus 4.8 fm in the out-of-plane direction, which is a 50% variation in path length. However, for central (0%–20%) collisions, the path length through the medium varies from 5.0 fm in the in-plane direction to 5.8 fm in the out-of-plane direction, which is a much smaller 16% variation. It is notable that the thickness through the medium in midcentral (20%–60%) collisions changes more with respect to the reaction plane than it does between central and midcentral collisions where the away-side suppression at large momentum is already known to vary [4]. Also worth noting is that the largest thickness in midcentral collisions is comparable to the shortest thickness in central collisions.

Any prediction for the away-side suppression with respect to the reaction plane will be a convolution of the energy loss and a description of the space-time evolution of the medium. In the limit where the medium is never fully opaque to fast partons and the energy lost by the typical parton is some fraction of its initial energy, the away-side suppression will increase with angle with respect to the reaction plane. This results because the average path length through the medium of the recoil parton is longer when out of the reaction plane. It is possible, in the extreme limit of a medium with a large opaque core and thin transparent corona, the away-side suppression could instead weaken as the trigger particle orientation varies from the in-plane to out-of-plane directions. The weakening in the thin corona scenario results from two effects; a larger relative number of scattering centers producing a pair of back-to-back final-state particles in the out-of-plane direction, but also the variation of the trigger particle multiplicity by angle with respect to the reaction plane. However, it is worth noting that a large core and thin corona is an extreme configuration. Variations within more realistic models of the away-side suppression will be intermediate between these extreme scenarios.

In this paper, we present azimuthal correlation measurements between pairs of neutral pion trigger particles (t) within $p_T^t = 4$–7 GeV/c and charged hadron associated partner particles (a) within $p_T^a = 3$–4, 4–5, and 5–7 GeV/c. These combinations of final-state particle momentum ranges have previously been shown to be dominated by jet fragmentation as they are above medium-induced two-particle correlations which contribute significantly at lower momenta [4,5]. The low momentum structures (the "ridge" and "shoulder") may be the result of parton-medium interactions (e.g., [15–18]) or global correlations from fluctuating initial conditions [19,20]. These fluctuations have substantially less impact at large pair momentum where the background contribution becomes small. In this study, as illustrated in Fig. 1, using only particles at large pair momentum, the away-side ($\Delta\phi \approx \pi$) suppression by trigger particle orientation with respect to the reaction plane ($\phi_s = \phi^t - \psi$) is presented as a probe of both the mechanism

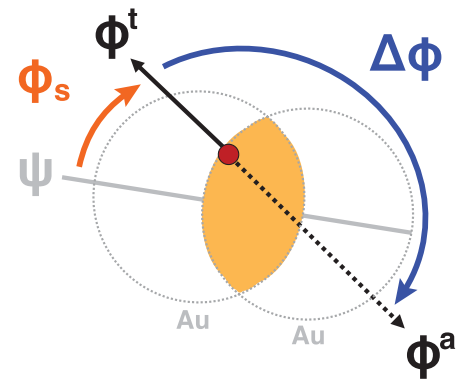

FIG. 1. (Color online) Definition of azimuthal angles. Trigger and associated partner particles are measured at ϕ^t and ϕ^a, respectively. The trigger particle orientations are taken with respect to the reaction plane $\phi_s = \phi^t - \psi$. The relative azimuthal separation of the trigger particle and the associated partner particle is $\Delta\phi = \phi^t - \phi^a$.

of parton energy loss and the space-time evolution of matter created by the collisions of large nuclei.

A previous measurement [21] by the STAR collaboration for midcentral (20%–60%) collisions between 4 and 6 GeV/c trigger particles and $2 < p_T^a < p_T^t$ GeV/c partner particles for two 45° wide in-plane and out-of-plane selections indicated an increased suppression of the away-side jet for the out-of-plane, but with little significance due to large underlying event subtraction uncertainties. The new results presented in our paper have sufficient statistics to specify a trend in the away-side suppression in midcentral (20%–60%) collisions at larger momentum where subtraction uncertainties are negligible.

II. EXPERIMENT

The results presented here are based on 3.4 billion minimum-bias Au + Au events recorded by the PHENIX detector in 2007. Comparisons to $p + p$ collisions use previously published measurements from data recorded in 2006 [5]. Collision centrality was determined by division into percentile of the integrated charge collected by beam-beam counters (BBC) [22] located at $|\eta|$ between 3.0 and 3.9. The timing between the arrival of charged particles in the north and south BBC was used to reconstruct the event position along the collision axis (z vertex), and to restrict the event sample to ±30 cm of the nominal interaction point of the two beams. The orientation of reaction-plane azimuthal angle (ψ) is reconstructed event-by-event using the quadrupole component (v_2) of the charge in the reaction plane (RXPN) detector [23], located at $|\eta|$ between 1.0 and 2.8. The resolution of the RXPN detector is highest (∼80%) for midcentral (20%–60%) collisions, where both the quadrupole component and the detector occupancy are large. The set of resolution corrections $\Delta_n : n \in \{2,\ 4,\ 6,\ 8\}$ for single particle anisotropies v_n where

$$v_n = \frac{v_n^{\text{obs}}}{\Delta_n} \tag{1}$$

are estimated from correlations between the independent north (ψ_N) and south (ψ_S) RXPN reaction-plane reconstructions [24,25]. A single fit parameter (x) is mapped into the resolution corrections via

$$\Delta_n = \frac{1}{2}\sqrt{\pi} x e^{-\frac{x^2}{2}} \left[I_{\frac{n/2-1}{2}}\left(\frac{x^2}{2}\right) + I_{\frac{n/2-1}{2}}\left(\frac{x^2}{2}\right)\right]. \tag{2}$$

The fit parameter is extracted from the correlations via:

$$C(\psi_N - \psi_S) = \frac{1}{2} e^{-\frac{x^2}{2}} \left\{ \frac{2}{\pi}\left(1 + \frac{x^2}{2}\right) + z[I_0(z) + L_0(z)] + \frac{x^2}{2}[I_1(z) + L_1(z)] \right\}, \tag{3}$$

where

$$z = \frac{x^2}{2}\cos(\psi_N - \psi_S). \tag{4}$$

The set of functions I_{2k} and L_{2k} are the even-ordered modified Bessel functions and the modified Struve functions, respectively.

The extracted values used to correct the measured second-order azimuthal anisotropy are $\Delta_2 = 0.66(4)$ and 0.66(3) for 0%–20% and 20%–60% centrality, respectively. Systematic uncertainties of 10% for 0%–5% centrality and 5% elsewhere account for nonflow contributions to the resolution corrections [23]. The similar values are a result of the peak in reaction-plane resolution appearing near 20% centrality. A direct inspection of these reaction-plane distributions for events containing a photon above 1 GeV/c did not reveal significant contributions from jets.

Neutral pion trigger particles are reconstructed from photon clusters measured by either lead-glass or lead-scintillator electromagnetic calorimeters (EMCal) in the two central arms of PHENIX, in total covering $|\eta| < 0.35$ and $2 \times 90°$ in azimuth [26]. Clusters are subject to cuts based on the known response of the EMCal, including removal of noisy and low-response towers, as well as shower shape cuts. Neutral pions are identified through the 2γ decay channel by pairing all photons within an event. Incorrect pairings between photons create a broad combinatorial background under the π^0 mass peak. This background is minimized by requiring the reconstructed mass to lie near the π^0 mass peak. This requirement was 0.125–0.160 MeV/c^2 for central events, but was relaxed to 0.120–0.165 MeV/c^2 in midcentral events where the combinatorial background is lower. Since combinatorial pairs are more often made with the abundant photons found at low energy, the energy asymmetry of the decay $[|E_1 - E_2|/(E_1 + E_2)]$ was restricted to be less than 0.5 for central (0%–5%) events. This was also relaxed for more peripheral events until all pairs with asymmetries less than 0.7 were accepted. The tightness of the cuts was used to control the rate of combinatorial pairings such that π^0 trigger particles have a signal-to-background ratio averaged over the mass window of 4:1 in central (0%–5%) collisions and 10:1 in midcentral (20%–60%) collisions.

Charged hadron partner particles are reconstructed in the central arms using the drift chambers (DC) with hit association requirements in two layers of multiwire proportional chambers with pad readout (PC1 and PC3), achieving a momentum resolution $\Delta p/p$ of $0.7\% \oplus 1.1\% p$ (GeV/c). Only tracks with unambiguous and distinguishable DC and PC1 hit information are used. Projections of these tracks are required to match a PC3 hit within a $\pm 2\sigma$ proximity window to reduce background from conversion and decay products. A track association to a signal in the ring imaging Čerenkov detector is used to reject electrons for partner selections below 5 GeV/c where little signal is produced by charged pions.

III. PAIR ANALYSIS

Within an event, all pairs formed from π^0 trigger particles (p_T^t = 4–7 GeV/c) and three sets of charged hadron associated partner particles (p_T^a = 3–4, 4–5, 5–7 GeV/c) are measured. Two centrality classes are used: central (0%–20%) and midcentral (20%–60%). Trigger particles are separated into six 15° bins in azimuthal angle with respect to the reaction plane $\phi_s = \phi^t - \psi$. The angular resolution of the measured reaction plane, at approximately 25°, is larger

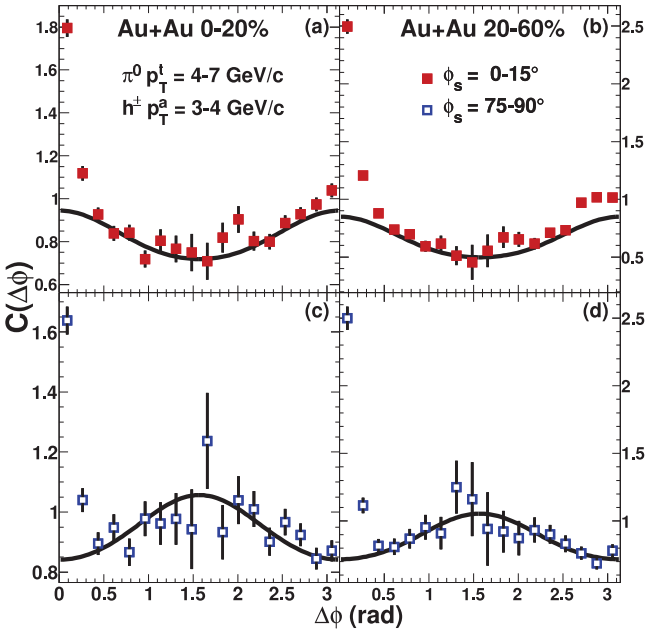

FIG. 2. (Color online) Correlation functions for (solid squares) the most in-plane, $\phi_s = 0$–15°, and (open squares) out-of-plane, $\phi_s = 75$–90°, trigger π^0 orientations in (left) central (0%–20%) and (right) midcentral (20%–60%) collisions for 3–4 GeV/c partner hadrons. Expected underlying event contributions are shown as solid curves (see text for details).

than this binning; consequently, significant smearing takes place between neighboring trigger orientation bins. Pairs within PHENIX are collected at different efficiencies due to the nonuniform central arm acceptance. The relative pair efficiencies are corrected by mixed pair distributions in which trigger and partner particles are drawn from different events of the same class (bins of 5% centrality, 5 cm z vertex). The resulting acceptance-corrected distributions are reported as correlation functions $C(\Delta\phi)$, which are defined as

$$C(\Delta\phi) = \frac{\frac{d\mathbb{m}^{ta}_{\rm same}}{d\Delta\phi}}{\frac{d\mathbb{m}^{ta}_{\rm mix}}{d\Delta\phi}} \frac{\int \frac{d\mathbb{m}^{ta}_{\rm mix}}{d\Delta\phi} d\Delta\phi}{\int \frac{d\mathbb{m}^{ta}_{\rm same}}{d\Delta\phi} d\Delta\phi}, \tag{5}$$

where $\mathbb{m}^{ta}$ is the number of measured pairs per event for either the same or mixed events, as indicated. Double-struck notation ($\mathbb{m}$) is used here to indicate measured quantities. Representative correlation functions for in-plane and out-of-plane trigger particle orientations are shown in Fig. 2. Note that these distributions are not corrected for reaction-plane resolution.

These inclusive pairs are assumed to correlate in one of two ways. (1) Two particles within the same event may correlate trivially by participation in the same collision geometry. These pairs produce an azimuthal angular correlation from the the single particle anisotropy with respect to the reaction plane. (2) Two particles may also correlate with each other via the same hard-scattering process. These particles will be fragments from the same (di)jet. To separate the jet particle pairs from the other background pairs, the two-source assumption is expressed as [27]

$$C(\Delta\phi) = J(\Delta\phi) + b_0\left[1 + \frac{\beta}{\alpha}\cos(2\Delta\phi) + \frac{\gamma}{\alpha}\cos(4\Delta\phi)\right], \tag{6}$$

where the jet contribution to the correlation function is contained in $J(\Delta\phi)$. The remaining harmonic terms describe the background contribution which is complicated by the trigger particle binning with respect to the reaction plane. The background modulation coefficients (α, β, γ) are calculated via

$$\alpha = 1 + 2v_2^t \cos(2\phi_s)\frac{\sin(2c)}{2c}\Delta_2 + 2v_2^t \cos(4\phi_s)\Delta_4, \tag{7}$$

$$\begin{aligned}\beta = {} & 2v_2^t v_2^a + 2v_2^a\left(1 + v_4^t\right)\cos(2\phi_s)\frac{\sin(2c)}{2c}\Delta_2 \\ & + 2v_2^t v_2^a \cos(4\phi_s)\frac{\sin(4c)}{4c}\Delta_4 \\ & + 2v_2^a v_4^t \cos(6\phi_s)\frac{\sin(6c)}{6c}\Delta_6,\end{aligned} \tag{8}$$

$$\begin{aligned}\gamma = {} & 2v_4^t v_4^a + 2v_4^a\left(1 + v_2^t\right)\cos(4\phi_s)\frac{\sin(4c)}{4c}\Delta_4 \\ & + 2v_2^t v_4^a\left[\cos(2\phi_s)\frac{\sin(2c)}{2c}\Delta_2 \cos(6\phi_s)\frac{\sin(6c)}{6c}\Delta_6\right] \\ & + 2v_4^t v_4^a \cos(8\phi_s)\frac{\sin(8c)}{8c}\Delta_8.\end{aligned} \tag{9}$$

This description of the background accounts for the trigger particle binning and reaction-plane resolution effects on the background shape [28]. The trigger particle orientation appears explicitly in terms of the bin center ϕ_s and width c. Single particle anisotropy values v_2 and v_4 were measured by correlating the trigger and partner particles with respect to the reaction plane, such that:

$$C(\phi - \psi) = 1 + 2v_2^{\rm obs}\cos[2(\phi - \psi)] + 2v_4^{\rm obs}\cos[4(\phi - \psi)], \tag{10}$$

where the observed anisotropies are corrected for the reaction-plane resolution as described previously in Eq. (1). Given sufficient detector resolution and narrowness of the trigger particle orientation binning, the sign of the $\cos(2\Delta\phi)$ term in Eq. (6) will flip sign between in-plane and out-of-plane bins as shown in Fig. 2. This effect is expected as selecting out-of-plane trigger particles should decrease the likelihood of finding a second background particle nearby. The same is not true for particles correlated via hard scattering. Both the second- and fourth-order anisotropy of the background correlations have been considered as the finite fourth-order contributions were determined to be nonnegligible for some trigger particle orientations. Likewise, higher order terms in the reaction-plane resolution correction are also included.

The uncertainties on the reaction-plane resolution corrections (Δ_n) and the observed anisotropies ($v_2^{\rm obs}$,$v_4^{\rm obs}$) are propagated separately as they impact the away-side suppression with respect to the reaction plane in characteristically different ways. The uncertainty in the reaction-plane resolution corrections is fully correlated between trigger orientations. For instance, this uncertainty increases (or decreases) both

the extracted in-plane and out-of-plane jet yields at $\Delta\phi = \pi$. However, the uncertainty in the observed anisotropies is fully anticorrelated between trigger orientations. Thus, this uncertainty increases the extracted in-plane yield while decreasing the out-of-plane yield (or vice versa). At large momentum, both of these subtraction uncertainties are small and always dominated by other sources. Recent measurements of odd anisotropies [29,30] have not be included as these contributions are subdominant to other sources of systematic uncertainty in these correlations between particles at large momenta.

The subtraction procedure was also examined for contamination of the jet correlations by fakes in the charged tracking, which become significant at large p_T. The fake high p_T tracks are present only in the partner sample and are largely uncorrelated with trigger particle for the partner p_T presented here. Thus the fake tracks, which are already less influential in events with a high p_T π^0, are subtracted with other uncorrelated pairs as part of the background contribution, so long as the anisotropies are measured with the same particle cuts. The subtraction robustness against tracking fakes at high p_T was checked by repeating the procedure with a 3σ PC3 matching requirement.

By taking the trigger particle orientation as $\phi_s = \pi/4$, the bin width as $c = \pi/2$, and by truncating higher than second-order terms, the functional form of the background in Eq. (6) reduces to the $v_2^t \times v_2^a$ modulation used in previous trigger particle orientation averaged results such as those found in [4]. This property is demonstrated in Fig. 3 where the trigger particles from all orientations are considered.

The background level b_0 is determined using the zero yield at minimum (ZYAM) method [27]. At high p_T the well-separated near- and away-side jets provide a large angular region at mid-$\Delta\phi$ angles with negligible jet signal. This allows the ZYAM level to be found with negligible bias and sufficient statistics despite the lower efficiency PHENIX has for collecting pairs near 90°. The ZYAM uncertainty was estimated through simulation of the statistical uncertainties as has been described in [31].

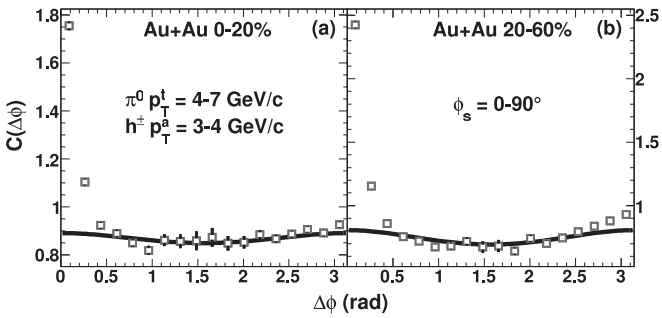

FIG. 3. Correlation functions for trigger π^0 averaged over all trigger orientations in central (0%–20%) and midcentral (20%–60%) collisions, left and right columns, respectively, for 3–4 GeV/c partner hadrons. Expected average underlying event contributions are shown as solid curves.

The jet contribution $J(\Delta\phi)$ is then reported as a per-trigger azimuthal yield such that:

$$\frac{1}{n^t}\frac{dn_{\rm jet}^{ta}}{d\Delta\phi} = \frac{1}{\epsilon^a}\frac{\mathbb{m}_{\rm same}^{ta}}{\mathbb{m}^t \int d\Delta\phi} J(\Delta\phi). \tag{11}$$

The efficiency-corrected single particle and pair rates are n^t and n^{ta}, respectively. The single particle partner efficiency ϵ^a is estimated in simulations of detector acceptance and occupancy as was done in [5]. By design, the trigger particle efficiency cancels in the ratio.

IV. RESULTS

Central (0%–20%) events are analyzed as a cross-check against experimental artifacts in midcentral (20%–60%) collisions since they have a smaller away-side jet yield. Thus, the central events should exhibit a smaller trigger particle angle variation, require a larger reaction-plane resolution correction, a larger event correlation subtraction, and have increased background in π^0 identification. Representative per-trigger azimuthal yields in central collisions for each of the partner momentum selections for the most in-plane and most out-of-plane trigger particle selections are shown in Fig. 4. The most in-plane and most out-of-plane trigger-particle orientations select the shortest and longest average path lengths through the medium, respectively, and thus may be expected to have the maximum differences.

On the near-side, a jet distribution is clearly observed for each selection. A direct comparison between the most in-plane and most out-of-plane trigger shows no significant variation. The measurement at mid-$\Delta\phi$ demonstrates the good agreement resulting from correct description of the underlying event correlations. On the away-side, the jet yield is small due to medium suppression and the statistical precision suffers once the pairs are divided among the various trigger particle orientations. No evidence of experimental artifacts such as over-subtraction or incorrect description of the background is seen, despite the challenging analysis environment present in central (0%–20%) collisions.

Integrated near- and away-side per-trigger yields (Y) are calculated within angular $\Delta\phi$ windows, as indicated in Fig. 4, approximating the 2σ width of the jet distributions measured in the trigger particle orientation averaged results. The near-side azimuthal integration windows are $\Delta\phi < \pi/9$ ($< 3\pi/18$) for $p_T^a > 4$ GeV/c (< 4 GeV/c). Similarly, the away-side azimuthal integrations windows are $\pi - \Delta\phi < 3\pi/18$ ($< 2\pi/9$) for $p_T^a > 4$ GeV/c (< 4 GeV/c). Use of these windows corresponds to an assumption that the jet distributions do not widen significantly at high p_T, as a function of the trigger particle orientation with respect to the reaction plane. This assumption is supported by the absence of significant centrality dependence in jet correlation widths ($\lesssim$20%) for particles at high p_T [5]. Within statistical uncertainties a constant jet width is consistent with the data. Integrated yields as a function of trigger particle orientation for both the near- and away-side are then corrected for the reaction-plane

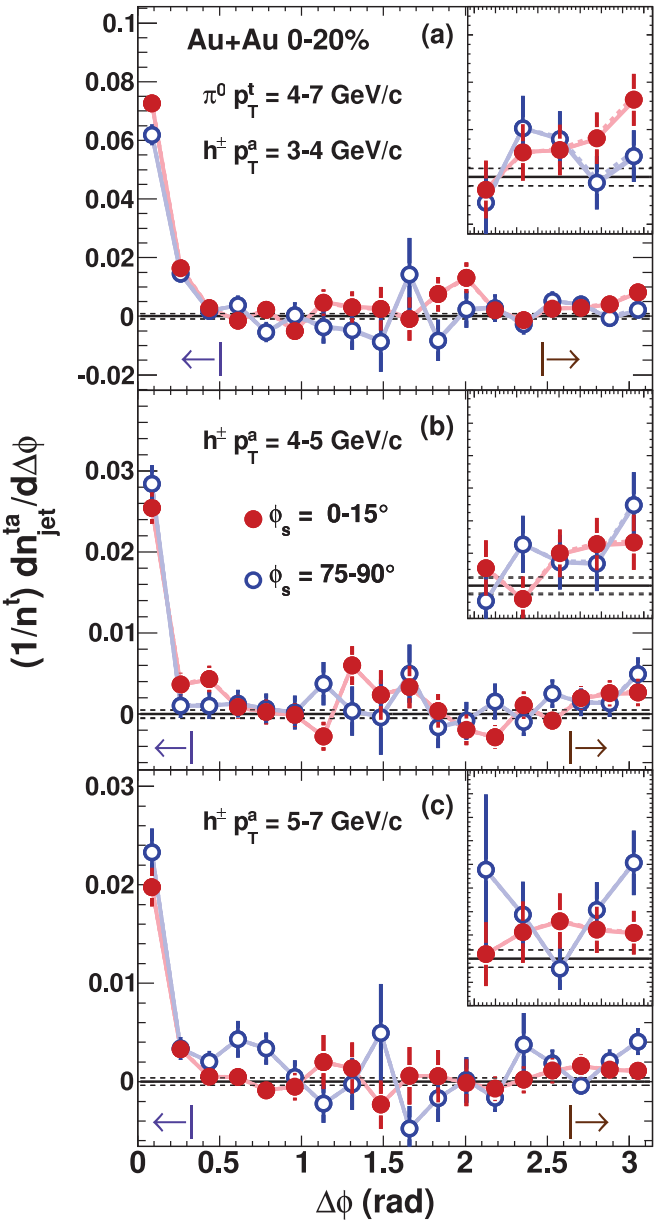

FIG. 4. (Color online) Per-trigger azimuthal jet yields for the most in-plane, $\phi_s = 0$–$15°$ (solid circles), and out-of-plane, $\phi_s = 75$–$90°$ (open circles), trigger particle selections in central (0%–20%) collisions for various partner momenta. Insets show away-side region on a zoomed scale. Bars indicate statistical uncertainties. Underlying event modulation systematic uncertainties are represented by bands through the points while the corresponding normalization uncertainties are shown as dashed lines around zero. Near- and away-side jet yield integration windows are indicated with arrows.

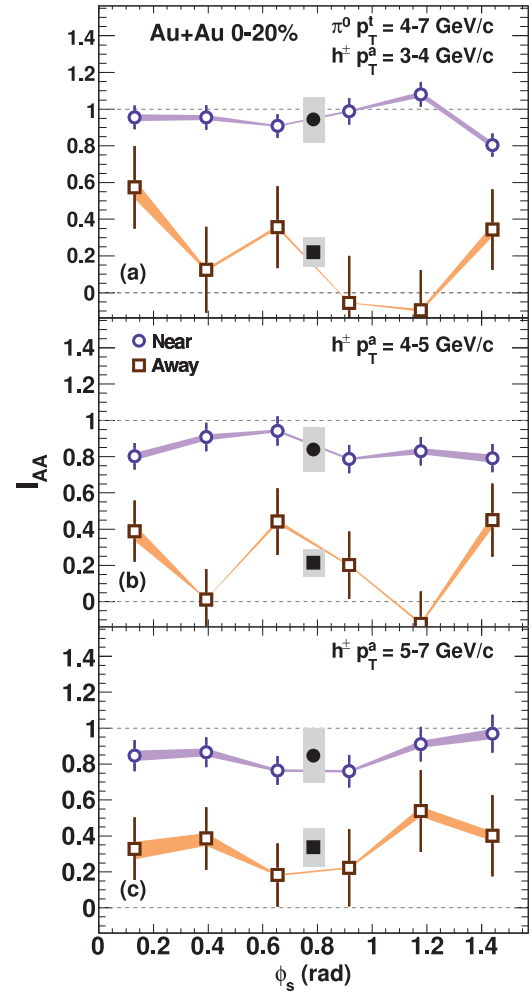

FIG. 5. (Color online) Nuclear jet suppression factor I_{AA} by angle with respect to the reaction plane ϕ_s for near- and away-side angular selections, circles and squares, respectively, in central (0%–20%) collisions for various partner momenta. Bars indicate statistical uncertainties. The shaded band shows the systematic uncertainty on the reaction-plane resolution unsmearing correction. Solid points show trigger particle angle averaged results and the global scale uncertainty.

resolution. The resolution correction is applied such that

$$Y(\phi_s) = \frac{1 + 2\left(v_2^{\mathrm{obs},Y}/\Delta_2\right)\cos(2\phi_s)}{1 + 2v_2^{\mathrm{obs},Y}\cos(2\phi_s)} Y_{\mathrm{meas}}(\phi_s), \qquad (12)$$

where Y and Y_{meas} are the corrected and uncorrected yields, respectively. The value of $v_2^{\mathrm{obs},Y}$ is the observed second-order anisotropy of integrated per-trigger yield with respect to the reaction plane and is determined by fitting the trigger particle orientation dependence of each $Y_{\mathrm{meas}}(\phi_s)$ measurement individually. This procedure is the similar to the correction of reaction-plane resolution on single particles, here applied to integrated per-trigger pair yields.

The corrected per-trigger yields (Y) are reported as the nuclear jet suppression with respect to $p + p$ collisions, $I_{\mathrm{AA}} = Y_{\mathrm{A+A}}/Y_{p+p}$. The result for central (0%–20%) collisions is shown in Fig. 5. The variation of the fit used in the resolution correction is the dominant source of ϕ_s-correlated uncertainty, having larger impact than the insignificant event anisotropy uncertainties. In the case of zero signal variation with reaction plane orientation, the correction becomes completely correlated with statistical scatter in the uncorrected measurement. Thus, the ϕ_s-correlated systematic uncertainty from the resolution correction is conservatively treated as correlated with the statistical uncertainty when computing the final significance of the measured trends. For the same reason,

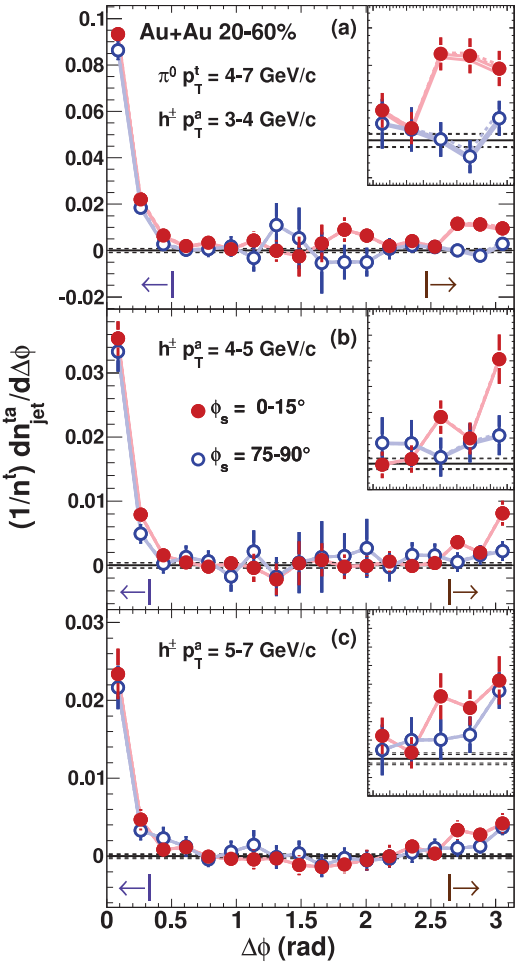

FIG. 6. (Color online) Per-trigger azimuthal jet yields for the most in-plane, $\phi_s = 0$–$15°$ (solid circles), and out-of-plane, $\phi_s = 75$–$90°$ (open circles), trigger particle selections in midcentral (20%–60%) collisions for various partner momenta. Insets show away-side region on a zoomed scale. Bars indicate statistical uncertainties. Underlying event modulation systematic uncertainties are represented by bands through the points while the corresponding normalization uncertainties are shown as dashed lines around zero. Near- and away-side jet yield integration windows are indicated with arrows.

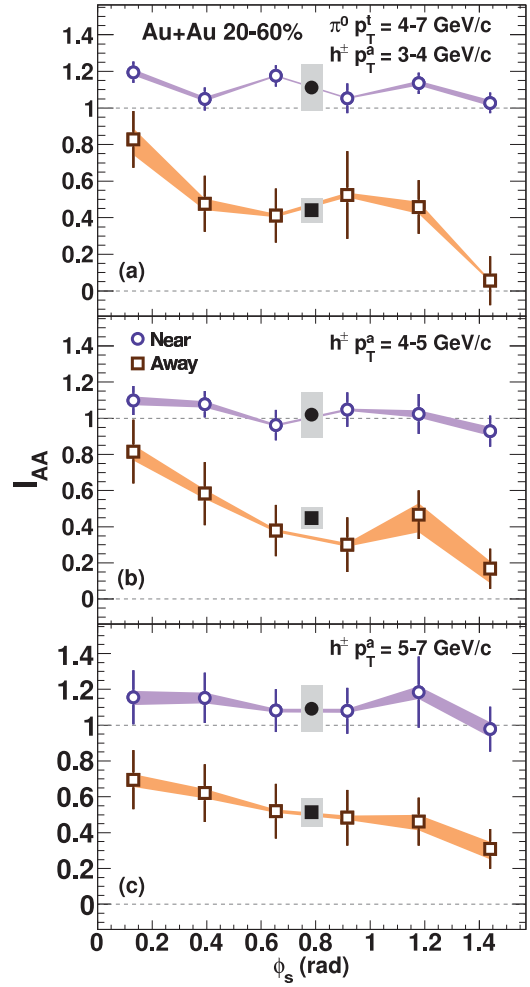

FIG. 7. (Color online) Nuclear jet suppression factor I_{AA} by angle with respect to the reaction plane ϕ_s for near- and away-side angular selections, circles and squares, respectively, in midcentral (20%–60%) collisions for various partner momenta. Bars indicate statistical uncertainties. The shaded band shows the systematic uncertainty on the reaction-plane resolution unsmearing correction. Solid points show trigger particle angle averaged results and the global scale uncertainty.

this source of systematic uncertainty has little correlation between the centrality and momentum selections.

For central events the near-side suppression is consistent with a constant as a function of ϕ_s within the statistical and ϕ_s-correlated systematic uncertainties. The values are also consistent with no suppression when considering the global scale uncertainty that appears on the trigger particle orientation averaged I_{AA}. On the away-side, there is significant suppression in central events, as evidenced by the trigger particle averaged I_{AA}, but the statistical precision with which to determine the ϕ_s variation is limited.

Midcentral (20%–60%) events, have greater eccentricity and could be expected to show correspondingly larger trigger particle orientation dependence due to path-length variation through the collision zone. The same set of representative per-trigger azimuthal yields is shown in Fig. 6 for the midcentral selection. Again, the near-side jets for the most in-plane and most out-of-plane trigger particle orientations are consistent with each other, a direct indication of little variation with respect to the reaction plane. The mid-$\Delta\phi$ are also in agreement with zero, as before, further demonstrating that the underlying event flow correlations are well described by Eqs. (6)–(9). In contrast to the near-side, the away-side measurements (see insets in Fig. 6) change between the in-plane and out-of-plane trigger particle orientations with the latter having consistently smaller yield for all partner momenta.

The integrated near- and away-side per-trigger jet yields for midcentral (20%–60%) collisions are shown in Fig. 7. The near-side jet is essentially flat, with negligible suppression [$I_{AA}(\phi_s) = 1$]. The away-side jet yield is increasingly suppressed with increasing ϕ_s. This falling trend results in only small associated particle yield remaining for out-of-plane trigger particle orientations.

In order to quantify the variation and significance of the trigger particle orientation dependencies shown in Figs. 5 and 7, the ratio of the out-of-plane to in-plane suppression (I_{AA}^{out}/I_{AA}^{in}) is constructed. In the ratio, the global scale uncertainties on each measurement cancel. The I_{AA} values at $\phi_s = 0^\circ$ (I_{AA}^{in}) and at 90° (I_{AA}^{out}) are estimated by both linear and flow-like cosine fits to the trigger particle angle measurements and evaluation at these angles. The reported ratios are therefore independent of the chosen binning with respect to the reaction plane and the values do not rely heavily on the assumed functional form of the dependence. The best-fit was determined by χ^2 minimization in which:

$$\tilde{\chi}^2 = \sum_i \left\{ \frac{[y_i + \epsilon_{sys}\sigma_{sys,i} - f(\phi_s)]^2}{\tilde{\sigma}_i^2(\epsilon_{sys})} \right\} + \epsilon_{sys}^2, \qquad (13)$$

where ϵ_{sys} is ± 1 for the $\pm 1\sigma_{sys}$ variation of the ϕ_s-correlated systematic uncertainty [32]. As discussed above, the systematic uncertainty is conservatively treated as fully correlated with the statistical uncertainty. The difference between linear and cosine fits provides only a small source of additional uncertainty due to the unknown true functional form. The resulting values of I_{AA}^{out}/I_{AA}^{in} and the total uncertainty are shown in Figs. 8 and 9. The average value of I_{AA}^{out}/I_{AA}^{in} across partner momentum is constructed by weighting the individual measurements by the $p + p$ per-trigger yields [5]. In general, the data are well fit by both the linear and cosine functions, giving reasonable χ^2. No evidence is seen for systematic deviations from either fit within the sizable statistical uncertainties and both forms give similar goodness of fit values. These values appear along with the I_{AA}^{out}/I_{AA}^{in} ratios in Table I.

For both central (0%–20%) and midcentral (20%–60%) collisions, the near-side jet yield is independent of trigger particle orientation with respect to the reaction plane within one standard deviation of the experimental uncertainties. These measurements are consistent with surface bias of the hard scattering center created by the requirement of a trigger particle and a resulting short path length through the collision zone traversed by the near-side parton. Central collisions have insufficient statistics to determine the away-side variation.

However in midcentral collisions where the expectation of surface bias would lead to a large variation in the path length traversed by the away-side parton, the measurements show a significant falling trend with increasing trigger particle angle with respect to the reaction plane. The suppression of away-side jet fragments in the out-of-plane direction is larger than in the in-plane direction, the out-of-plane away-side jet peak having only $(26 \pm 20)\%$ of the yield of the in-plane direction. Thus the large variation by angle with respect to the reaction plane is significant. Assuming the modulation to be flow-like (dominated by the second-order variation), the suppression pattern implies $v_2^{I_{AA}} = 0.29^{+0.15}_{-0.11}$. As the midcentral away-side measurements are consistent between p_T^a selections within the stated uncertainties, the hint of a rising trend in p_T^a is not significant. The values quoted here are consistent with those previously measured in [21] and provide a factor of 4 better constraint in the I_{AA}^{out}/I_{AA}^{in} ratio.

Recent single particle measurements of azimuthal anisotropy at high p_T (6–9 GeV/c) found that $v_2 = 0.13 \pm 0.01 \pm 0.01$ [9]. Thus, the away-side per-trigger yields at high p_T favor an anisotropy larger than that measured for the single

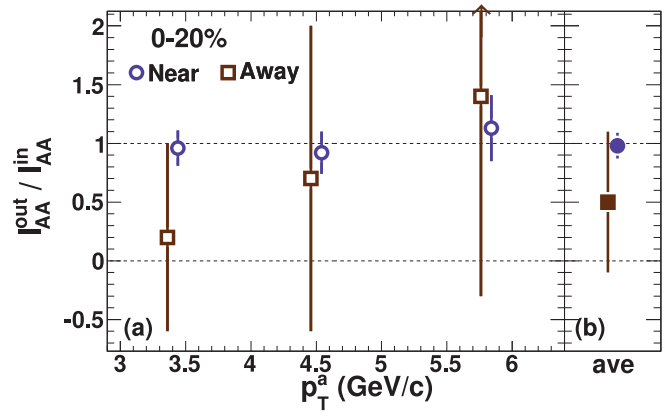

FIG. 8. (Color online) Angle with respect to the reaction-plane dependence of the nuclear suppression factor I_{AA} expressed as the ratio between in-plane and out-of-plane trigger particles from fits to the data in central (0%–20%) collisions. The bars represent total uncertainty taking into account the correlations between sources (see text for details).

TABLE I. Angle with respect to the reaction-plane dependence of the nuclear suppression factor I_{AA} expressed as the ratio between in-plane and out-of-plane trigger particles from linear and cosine fits to the data (see text for details). The total uncertainty taking into account the correlations between sources is reported.

Selection		Near-side					Away-side				
Cent	p_T^a	linear		cosine		average	linear		cosine		average
		I_{AA}^{out}/I_{AA}^{in}	χ^2/dof	I_{AA}^{out}/I_{AA}^{in}	χ^2/dof		I_{AA}^{out}/I_{AA}^{in}	χ^2/dof	I_{AA}^{out}/I_{AA}^{in}	χ^2/dof	
0%–20%	3–4	0.95 ± 0.15	9.5/4	0.96 ± 0.15	10.0/4	0.96 ± 0.15	0.1 ± 0.7	5.0/4	0.2 ± 0.8	5.1/4	0.2 ± 0.8
	4–5	0.92 ± 0.18	3.0/4	0.92 ± 0.16	3.0/4	0.92 ± 0.18	0.7 ± 1.3	9.0/4	0.6 ± 1.2	8.7/4	0.7 ± 1.3
	5–7	1.15 ± 0.30	3.1/4	1.10 ± 0.26	3.3/4	1.13 ± 0.28	1.5 ± 2.0	2.0/4	1.3 ± 1.4	1.8/4	1.4 ± 1.7
	3–7	–	–	–	–	0.98 ± 0.11	–	–	–	–	0.5 ± 0.6
20%–60%	3–4	0.90 ± 0.14	5.0/4	0.92 ± 0.12	5.5/4	0.91 ± 0.13	0.15 ± 0.25	4.0/4	0.25 ± 0.38	5.5/4	0.20 ± 0.32
	4–5	0.85 ± 0.17	1.2/4	0.88 ± 0.15	1.5/4	0.87 ± 0.16	0.20 ± 0.20	3.0/4	0.30 ± 0.35	4.0/4	0.25 ± 0.28
	5–7	0.88 ± 0.28	0.5/4	0.88 ± 0.21	0.7/4	0.88 ± 0.25	0.40 ± 0.30	0.3/4	0.50 ± 0.30	0.5/4	0.45 ± 0.30
	3–7	–	–	–	–	0.89 ± 0.10	–	–	–	–	0.26 ± 0.20

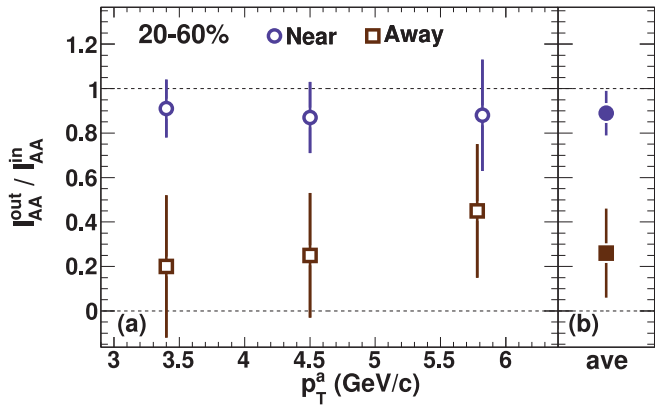

FIG. 9. (Color online) Angle with respect to the reaction-plane dependence of the nuclear suppression factor I_{AA} expressed as the ratio between in-plane and out-of-plane trigger particles from fits to the data in midcentral (20%–60%) collisions. The bars represent total uncertainty taking into account the correlations between sources (see text for details).

particles. However, the difference is marginal and additional measurements will be needed to confirm.

Shown in Fig. 10 are the results of a Monte Carlo energy loss calculation from Renk [33,34] using the time-space evolution provided by two different hydrodynamic simulations [35,36] and two initial state descriptions, Glauber and CGC. These particular combinations of a jet energy loss model and collision evolution together predict less variation in the away-side suppression with respect to the reaction plane than is witnessed by the data. Variation of the initial geometry description within [35] between Glauber and CGC produces only small changes in the extracted I_{AA} out-of-plane to in-plane ratio, indicating limited sensitivity to this model parameter of the reaction plane dependent dijet observable. However, other model parameters

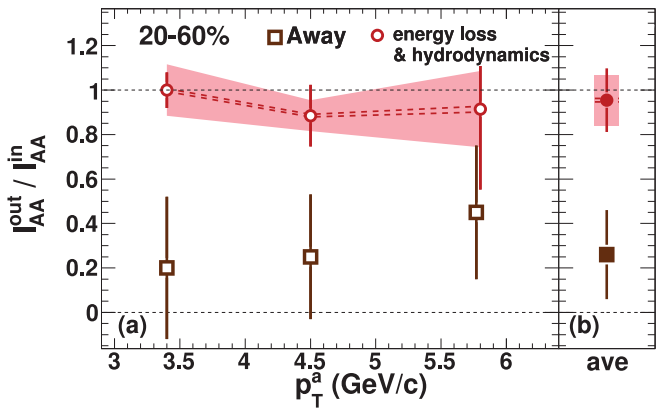

FIG. 10. (Color online) Away-side I_{AA}^{out}/I_{AA}^{in} ratio for midcentral (20%–60%) collisions, from Fig. 9 (squares). The average result from an energy loss calculation [33,34] using two hydrodynamic evolution models [35,36] (circles) and the associated Monte Carlo statistical uncertainties. The shaded band shows the uncertainty that results from the selection of a particular hydrodynamic evolution; the lower extent covering [35] and the upper covering [36]. Dotted lines show the small uncertainty resulting from the initial event geometry (Glauber or CGC) as calculated within [35].

that vary between the two hydrodynamic models (such as the thermalization time and freeze-out temperature) were found to impact the away-side suppression anisotropy to a greater degree, indicating sensitivity to simulation parameters that are not well-constrained by other measurements. Consequently, these data warrant more detailed study with various energy loss models, and also different space-time evolution models. Model comparisons would also benefit from improved measurement precision. While additional RHIC runs with the current detector will provide an increase in the available statistics, the precision of this result will be dramatically improved, as is needed for central collisions, with an upgraded PHENIX detector.

V. SUMMARY

We have shown that away-side jet fragment suppression increases substantially with increasing angle with respect to the reaction plane in 20%–60% Au + Au collisions at $\sqrt{s_{NN}} = 200$ GeV. The away-side yield in the out-of-plane orientation is reduced by a factor of ∼4 relative to the in-plane direction. In contrast, the measured near-side I_{AA} is reaction plane independent, and consistent with no suppression. These results directly show that the energy lost by fast partons in the hot nuclear medium increases as their paths through the medium become long. A theoretical description of these experimental data implementing an energy loss formalism and a time-space evolution of the collision should be sought in union with other experimental quantities; such as R_{AA}, I_{AA}, and $R_{AA}(\phi_s)$ [2,4,5,25,37]. Energy loss formalisms that have successfully described the large momentum R_{AA} and I_{AA} may be paired with a particular time-space evolution in also describing the ϕ_s dependence of these same quantities. As shown for the combination above, the data presented here disagree with the present calculations. These data should play an important role in constraining simulations of the space-time evolution of heavy-ion collisions and the subsequent extraction of medium properties.

ACKNOWLEDGMENTS

We thank the staff of the Collider-Accelerator and Physics Departments at Brookhaven National Laboratory and the staff of the other PHENIX participating institutions for their vital contributions. We acknowledge support from the Office of Nuclear Physics in the Office of Science of the Department of Energy, the National Science Foundation, a sponsored research grant from Renaissance Technologies LLC, Abilene Christian University Research Council, Research Foundation of SUNY, and Dean of the College of Arts and Sciences, Vanderbilt University (USA), Ministry of Education, Culture, Sports, Science, and Technology and the Japan Society for the Promotion of Science (Japan), Conselho Nacional de Desenvolvimento Científico e Tecnológico and Fundação de Amparo à Pesquisa do Estado de São Paulo (Brazil), Natural Science Foundation of China (People's Republic of China), Ministry of Education, Youth and Sports (Czech Republic), Centre National de la Recherche Scientifique, Commissariat à l'Énergie Atomique, and Institut National de Physique

Nucléaire et de Physique des Particules (France), Ministry of Industry, Science and Tekhnologies, Bundesministerium für Bildung und Forschung, Deutscher Akademischer Austausch Dienst, and Alexander von Humboldt Stiftung (Germany), Hungarian National Science Fund, OTKA (Hungary), Department of Atomic Energy and Department of Science and Technology (India), Israel Science Foundation (Israel), National Research Foundation and WCU program of the Ministry Education Science and Technology (Korea), Ministry of Education and Science, Russia Academy of Sciences, Federal Agency of Atomic Energy (Russia), VR and the Wallenberg Foundation (Sweden), the US Civilian Research and Development Foundation for the Independent States of the Former Soviet Union, the US-Hungarian Fulbright Foundation for Educational Exchange, and the US-Israel Binational Science Foundation.

[1] K. Adcox *et al.*, Nucl. Phys. A **757**, 184 (2005).
[2] S. S. Adler *et al.*, Phys. Rev. C **76**, 034904 (2007).
[3] J. Adams *et al.*, Phys. Rev. Lett. **97**, 162301 (2006).
[4] A. Adare *et al.*, Phys. Rev. C **78**, 014901 (2008).
[5] A. Adare *et al.*, Phys. Rev. Lett. **104**, 252301 (2010).
[6] C. Loizides, Eur. Phys. J. C **49**, 339 (2007).
[7] T. Renk and K. J. Eskola, Phys. Rev. C **75**, 054910 (2007).
[8] F. Dominguez, C. Marquet, A. H. Mueller, B. Wu, and B.-W. Xiao, Nucl. Phys. A **811**, 197 (2008).
[9] A. Adare *et al.*, Phys. Rev. Lett. **105**, 142301 (2010).
[10] S. A. Bass, C. Gale, A. Majumder, C. Nonaka, G.-Y. Qin, T. Renk, and J. Ruppert, Phys. Rev. C **79**, 024901 (2009).
[11] S. Wicks, W. Horowitz, M. Djordjevic, and M. Gyulassy, Nucl. Phys. A **784**, 426 (2007).
[12] M. L. Miller, K. Reygers, S. J. Sanders, and P. Steinberg, Annu. Rev. Nucl. Part. Sci. **57**, 205 (2007).
[13] H.-J. Drescher and Y. Nara, Phys. Rev. C **75**, 034905 (2007).
[14] M. Luzum and P. Romatschke, Phys. Rev. C **78**, 034915 (2008).
[15] J. Casalderrey-Solana, E. V. Shuryak, and D. Teaney, arXiv:hep-ph/0602183.
[16] S. S. Gubser, S. S. Pufu, and A. Yarom, Phys. Rev. Lett. **100**, 012301 (2008).
[17] I. Vitev, Phys. Lett. B **630**, 78 (2005).
[18] A. D. Polosa and C. A. Salgado, Phys. Rev. C **75**, 041901 (2007).
[19] P. Sorensen, arXiv:0808.0503.
[20] J. Takahashi *et al.*, Phys. Rev. Lett. **103**, 242301 (2009).
[21] J. Adams *et al.*, Phys. Rev. Lett. **93**, 252301 (2004).
[22] M. Allen *et al.*, Nucl. Instrum. Methods A **499**, 549 (2003).
[23] E. Richardson *et al.*, Nucl. Instrum Meth. A **636**, 99 (2011).
[24] S. Afanasiev *et al.*, Phys. Rev. C **80**, 024909 (2009).
[25] S. Afanasiev *et al.*, Phys. Rev. C **80**, 054907 (2009).
[26] A. Adare *et al.*, Phys. Rev. Lett. **101**, 232301 (2008).
[27] S. S. Adler *et al.*, Phys. Rev. Lett. **97**, 052301 (2006).
[28] J. Bielcikova, S. Esumi, K. Filimonov, S. Voloshin, and J. P. Wurm, Phys. Rev. C **69**, 021901 (2004).
[29] A. Adare *et al.*, arXiv:1105.3928.
[30] K. Aamodt *et al.*, Phys. Rev. Lett. **107**, 032301 (2011).
[31] A. Sickles, M. P. McCumber, and A. Adare, Phys. Rev. C **81**, 014908 (2010).
[32] A. Adare *et al.*, Phys. Rev. C **77**, 024912 (2008).
[33] T. Renk, Phys. Rev. C **78**, 034904 (2008).
[34] T. Renk (private communication).
[35] C. Nonaka and S. A. Bass, Phys. Rev. C **75**, 014902 (2007).
[36] K. J. Eskola, H. Honkanen, H. Niemi, P. V. Ruuskanen, and S. S. Räsänen, Phys. Rev. C **72**, 044904 (2005).
[37] A. Adare *et al.*, Phys. Rev. C **80**, 024908 (2009).